# Optical properties of silicon nanocrystals covered by periodic array of gold nanowires

S. A. Dyakov,[1,2,*] D. M. Zhigunov,[3] A. Marinins,[1] M. R. Shcherbakov,[3] A. A. Fedyanin,[3] A. S. Vorontsov,[3] P. K. Kashkarov,[3,4] S. Popov,[1] M. Qiu,[5,1] M. Zacharias,[6] S. G. Tikhodeev,[7,3] and N. A. Gippius[2]

[1]*Department of Materials and Nano Physics, School of Information and Communication Technology, KTH Royal Institute of Technology, Electrum 229, 16440 Kista, Sweden*

[2]*Skolkovo Institute of Science and Technology, 143025 Moscow Region, Russia*

[3]*Faculty of Physics, M.V. Lomonosov Moscow State University, 119991 Moscow, Russia*

[4]*National Research Centre Institute", pl. Akademika Kurchatova 1, 123182 Moscow, Russia*

[5]*State Key Laboratory of Modern Optical Instrumentation, Department of Optical Engineering, Zhejiang University, 310027 Hangzhou, China*

[6]*IMTEK, Faculty of Engineering, Albert-Ludwigs-University Freiburg, 79110 Freiburg, Germany*

[7]*A. M. Prokhorov General Physics Institute, RAS, Vavilova 38, Moscow, Russia*

(Received 27 February 2016; revised manuscript received 8 April 2016; published 6 May 2016)

Extinction and photoluminescence spectra are experimentally and theoretically studied for a periodic array of gold nanowires deposited on top of a dielectric substrate containing silicon nanocrystals. Quasiguided modes are observed in the substrate resulting in modification of optical properties of silicon nanocrystals. Our calculations of extinction and photoluminescence spectra are in good agreement with experimental results. The periodicity provides a powerful tool for achieving a high photoluminescence outcoupling efficiency of silicon nanocrystals.

DOI: 10.1103/PhysRevB.93.205413

## I. INTRODUCTION

The light-matter interaction in materials can be efficiently manipulated by periodic structuring on a submicrometer scale. In particular, photonic crystal slabs attract great attention from researchers due to the ample opportunities to control the radiation field of emitters [1–4]. Silicon nanocrystals (NCs) are known to be compatible with silicon-based technology and to exhibit room-temperature photoluminescence, which makes them promising for solar cell and optoelectronic applications.

In the literature there are a lot of papers dedicated to the modification of photoluminescence properties of silicon nanocrystals due to different dielectric environments [5–15]. In general, the photoluminescence of molecules or quantum dots, which are placed into a nonhomogeneous dielectric environment, can be enhanced or suppressed depending on the combination of several factors.

The first factor is a local excitation field. Since the excitation field is distributed within the structure inhomogeneously and the excitation transfer between different nanocrystals is negligibly small [16], the local photoluminescence intensity appears to be a function of the coordinates of the emitter. It was shown experimentally in Ref. [10] that due to this effect, one can twentyfold increase the photoluminescence intensity of all-dielectric structures with silicon nanocrystals by a proper choice of the excitation wavelength and the thicknesses of the buffer and emitting layers. Besides, the excitation local field effects is the main mechanism in plasmonic enhancement of silicon nanocrystals photoluminescence [5,8,9,15,17]. The second factor that can change the photoluminescence properties of molecules or quantum dots is the influence of the dielectric environment of an emitter on the outcoupling efficiency, i.e., a portion of the emitted light that comes out from the sample and reaches the detector. According to the electrodynamic reciprocity principle, this phenomenon is similar to the local excitation field effect but happens, generally speaking, at different frequency. For silicon nanocrystals, the effect of modulation of outcoupling efficiency was studied in Refs. [10–12,14,18,19]. Additionally, the dielectric environment of emitters can modify their radiative recombination rate in accordance with Fermi's golden rule.

The influence of a hosting matrix ($SiO_2$) on the spontaneous emission rate can be described in terms of a so-called Purcell factor. This influence was experimentally demonstrated for silicon nanocrystals and successfully theoretically described in Refs. [6,13]. In the presence of a metal, the probability of nonradiative relaxation of an excited state is also modified. It can be shown [17] that when a metal nanoparticle is approaching a semiconductor quantum dot, the nonradiative spontaneous decay rate grows and the approximation of oscillating point dipole breaks down [20]. Such luminescence quenching is discussed in Refs. [5,8,9,15,17].

In spite of the rather large number of publications devoted to optical properties of silicon nanocrystals, it is important to look into the opportunity for photoluminescence intensity engineering based on the use of metal nanostructures. In this paper we aim to experimentally and theoretically study of the optical properties of silicon nanocrystals covered by a one-dimensional array of gold nanowires, which provide an excitation of quasiguided modes [21,22].

The structure of the paper is as follows. Section II is dedicated to the experimental and theoretical methods used in this work. In Secs. III A, B, and C we experimentally and theoretically analyze the extinction spectra of the structure under study and show that silicon nanocrystals form an effective layer, which acts as a waveguide. In Sec. III D, we demonstrate the silicon nanocrystals photoluminescence enhancement and explain the mechanisms of this phenomenon in detail.

*sedyakov@kth.se

 

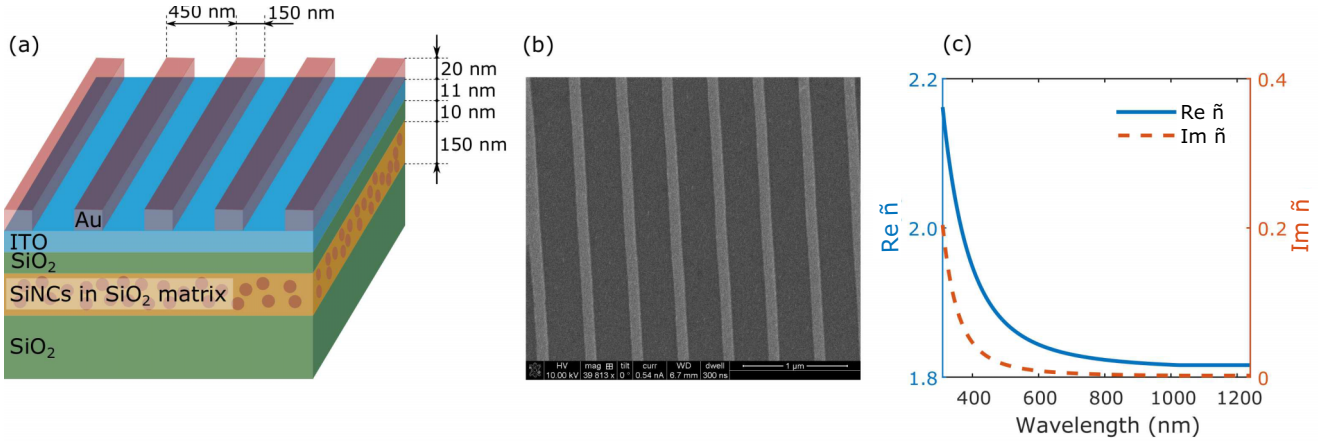


FIG. 1. (a) Schematic view of sample with silicon nanocrystals and gold grating. Silicon nanocrystals are shown by circles. (b) SEM image of the structure under study. (c) Experimental real and imaginary parts of effective refractive index of the layer with silicon nanocrystals.

## II. METHODS

### A. Structure and experimental details

The schematic view of the experimental sample is shown in Fig. 1(a). The structure consists of a periodic array of gold nanowires deposited on a $SiO_2$ substrate, which contains silicon nanocrystals. The gold nanowires have a width of 150 nm, a height of 20 nm, and a pitch size of 450 nm. Silicon nanocrystals are evenly distributed in the $SiO_2$ substrate on the depths from 10–160 nm. The SEM image of the sample is shown in Fig. 1(b).

Reactive evaporation of SiO powder in an oxygen-controlled atmosphere was used to deposit multilayered $SiO/SiO_2$ films on quartz substrates. Each film consisted of alternating SiO and $SiO_2$ layers with the thicknesses of 1.5 and 4 nm, respectively. After the deposition the conventional tube furnace annealing for one hour in $N_2$ atmosphere was used in order to fabricate Si nanocrystals arrays (for details see Ref. [23]).

The gold nanowires deposition procedure is as follows. First, the glass substrate with silicon nanocrystals is covered by 11-nm thick indium tin oxide (ITO) layer as an adhesion promoter between gold and silica. Then, the sample is cleaned in an ultrasonic bath with acetone (10 min) and isopropanol (10 min), then $N_2$ blow dried. Next, Microchem polymethylmethacrylate A4 positive photoresist is spincoated at 3000 rates per minute for 45 s and prebaked at 170 °C for 1 min forming a 250-nm thick uniform layer. Then, e-beam exposure acceleration voltage is performed at 25 kV with a Raith 150 high-resolution lithography system to pattern the grating lines. After development in methylisobutylketone-isopropanol (MIBK:IPA) 1:3 solution (45 s) and rinsing in IPA (15 s) the sample is sent to a Eurovac e-gun evaporation system to deposit 20 nm of Au. After Au deposition is finished, the lift-off process is performed by immersing the sample in acetone. This removes the photoresist with the excess Au leaving only Au grating lines deposited on ITO, which serves as a transparent adhesion promoter.

Transmittance spectra are measured as a function of the angle of light incidence. In the setup, light from a broadband source (50 W halogen lamp) is collimated and slightly focused to a spot of ca 500 $\mu$m in diameter. The polarization state is controlled by a GlanTaylor linear polarizer. The transmitted beam is collected and sent to a compact CCD-based visible spectrometer. The sample is held by a three-axis holder that allows for the control of the incidence angle with a step of 1°. Spectra are measured consecutively for the sample area and the substrate without gold grating; then, the sample spectra are normalized over the substrate spectra.

Photoluminescence (PL) spectra were registered under the 337 nm $N_2$ laser line excitation using 500 mm single-grating spectrometer equipped with an air-cooled CCD camera. The spectra were taken at room temperature and were corrected for the system response.

### B. Theoretical methods

For the theoretical study of optical properties of the structures described above we calculate their extinction spectra, emissivity spectra, as well as the dispersion relation of the waveguide and quasiguided modes in the empty lattice approximation.

The presence of silicon nanocrystals in the substrate causes light scattering as well as light absorption at the surface defects and energy levels of silicon nanocrystals. This situation is quite different from that when electromagnetic waves pass through a bare $SiO_2$ without significant absorption. In simulations, we account for the influence of silicon nanocrystals on light propagation by introducing a homogeneous layer of a certain effective refractive index. The thickness of this layer is chosen as 150 nm, which provides the best agreement between measured and calculated spectra. The effective refractive index spectrum is measured using the ellipsometry technique and takes the imaginary part into account [see Fig. 1(c)].

Simulations of extinction spectra are performed by the scattering matrix method [24,25]. The general idea of this method is the Fourier decomposition of the electromagnetic field into planar waves with different projections of the momentum vector onto the direction of periodicity. In order to achieve a better convergence with respect to the number of plane waves, we employ the factorization rules [26].

The intensity of photoluminescence is calculated as a power emitted by the oscillating electric dipoles evenly distributed

over the layer with silicon nanocrystals. The resulted PL intensity accounts for the contribution from all dipoles:

$$I = \sum_i I_i. \quad (1)$$

The emitted power of each dipole is calculated as a product of an excitation efficiency and an outcoupling efficiency. The excitation efficiency is taken as a square of the absolute value of complex amplitude of the electric field of excitation light at the position of the dipole. Due to the inhomogeneous excitation field distribution within the active layer and the absence of excitation transfer between different nanocrystals, all the dipoles have different excitation efficiencies. The outcoupling efficiency is calculated in assumption of unit dipoles oscillation amplitude and has a meaning of a power that is emitted by the dipole and outcouples to the far field. The far-field outcoupling efficiency is calculated using the electrodynamic reciprocity principle. According to this principle the currents of two different dipoles $j_{1,2}$ and their electric fields $E_{1,2}$ at the positions of the other dipole are connected as $j_1 E_2 = j_2 E_1$. This enables us to predict the far-field emission characteristics by calculating the near-field distribution of the plane wave, which is coming in from the far field. As a result, the problem of simulation of photoluminescence intensity is reduced to the calculation of electric field of a plane wave, which hits the sample from the far field:

$$I \sim \sum_i |\mathbf{E}_{\mathrm{exc}}(\hbar\omega_{\mathrm{exc}}, \mathbf{k}_{\|\mathrm{exc}}, \mathbf{r}_i)|^2 \times |\mathbf{E}_{\mathrm{pl}}(\hbar\omega_{\mathrm{pl}}, \mathbf{k}_{\|\mathrm{pl}}, \mathbf{r}_i)|^2, \quad (2)$$

where $\mathbf{E}_\alpha$ is the electric vector, $\hbar\omega_\alpha$ is the photon energy, $\mathbf{k}_{\|\alpha} \equiv (k_{x\alpha}, k_{y\alpha})$ is the in-plane projection of photon quasimomentum vector, symbol $\alpha =$ exc or $pl$ relates to the excitation or photoluminescence, and $\mathbf{r}_i \equiv (x_i, z_i)$ is the coordinate of oscillating dipole.

In order to understand the energy dispersion of electromagnetic resonances in the structure, we used the empty-lattice approximation [24]. In this approximation, the dispersion relation is calculated for the new effective structure consisting of ITO/$SiO_2$/SiNCs waveguide and the metallic grating is replaced by a homogeneous layer of gold. The energy dispersion curves are found as the solution of transcendental equation $\det S^{-1}(\omega, k_x) = 0$, where $S$ is the scattering matrix of the effective structure with an empty lattice, which can be represented in the form of a $2 \times 2$ matrix. To introduce the surface periodicity, the obtained dispersion curves are then folded back on the $\omega$-$k_x$ diagram into the first Brillouin zone.

## III. RESULTS

### A. Dispersion relations in the empty-lattice approximation

The layer of silicon nanocrystals supports the waveguide modes even without periodicity that is provided by the gold grating. These modes are below the light line so that no plane electromagnetic wave traveling from the far field can satisfy the energy-momentum conservation laws and couple to the waveguide.

The dispersion relations of the lowest waveguide modes of the silicon nanocrystals layer are calculated in the empty lattice approximation for TM and TE polarizations and shown in Fig. 2(a). The folded quasiguided modes are displayed in Fig. 2(b). The corrugation period $a$ determines the position of the modes at $k_x = 0$.

The empty lattice approximation qualitatively figures out the behavior of guided modes in the structure with periodic gold grating. This approximation, however, is unable to predict

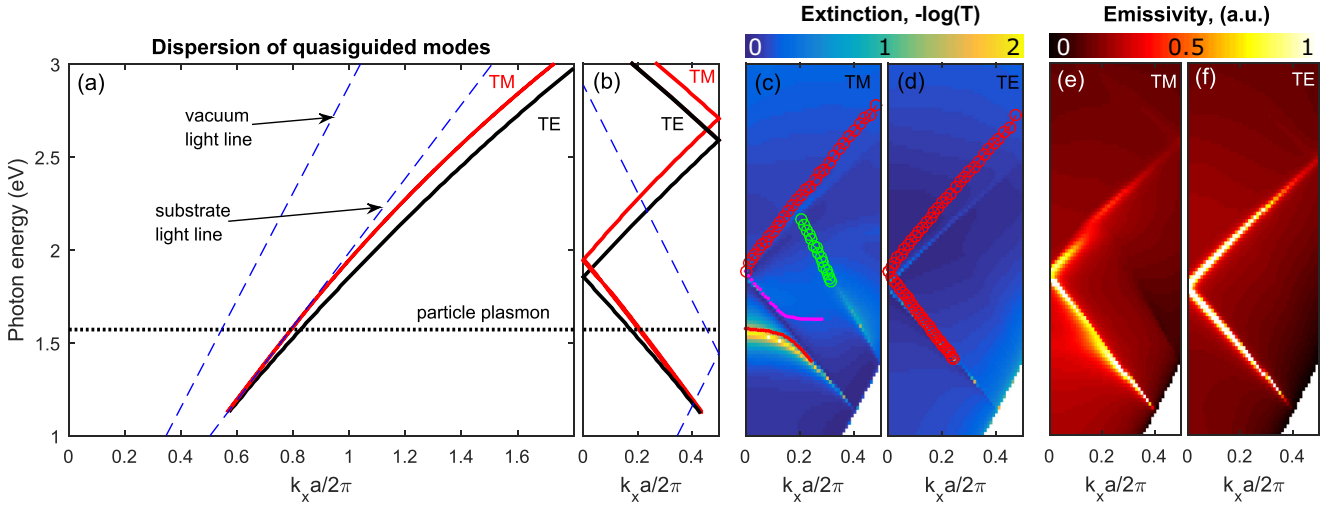


FIG. 2. (a) The calculated dispersions of the TE and TM quasiguided modes in the empty lattice approximation. The dashed lines represent the vacuum and substrate light lines. The dotted line shows the spectral position of localized surface plasmon. (b) The dispersion folded into the first Brillouin zone. (c)–(d): Extinction $[-\log(T)]$ of structures with active layer of silicon nanocrystals as a two-dimensional function of photon energy and $k_x$ calculated for (c) TM polarized light and (d) TE polarized light. Red circles represent the experimentally observed quasiguided modes, green circles shows Rayleigh anomalies, and magenta dots represent the hybrid waveguide plasmon mode. The colored scheme is explained on the color bar. (e)–(f): Intensity of light outcoupled from structures with an active layer of silicon nanocrystals as a two-dimensional function of photon energy $E$ and $x$ component of the wave vector $k_x$ calculated for the (e) TM polarized light and (f) TE polarized light. The colored scheme is explained on the color bar.

the spectral position of localized surface plasmon (particle plasmon) associated with the individual gold nanowires. As it will be shown below, the frequency of the localized surface plasmons can be calculated by the scattering matrix method. In Fig. 2, the flat dispersion of the particle plasmons in individual gold nanowires is shown by the horizontal dotted line.

In what follows it will be shown that the dispersion of the quasiguided modes in the first Brillouin zone defines the behavior of resonances in extinction and photoluminescence spectra [see Figs. 2(c)–2(f)].

### B. Extinction spectra: theory and experiment

Experimental and theoretical extinction spectra of the sample are shown in Fig. 3 for TM polarization and in Fig. 4 for TE polarization. From top to bottom, the polar angle of incidence is increased from 0° to 30°, while the azimuthal angle $\phi = 0°$ remains unchanged. All extinction spectra exhibit pronounced spectral features with distinct dependence on the angle of incidence. It can be seen in Fig. 3(a) that the TM extinction spectrum at normal incidence has two peaks. As it will be shown later, the more pronounced peak, at $\approx 1.57$ eV, is associated with a localized surface plasmon resonance in individual nanowires. The less pronounced one, at $\approx 1.977$ eV, arises due to appearance of quasiguided mode, which becomes optically active by introducing a periodicity in the system. A detailed analysis of the displayed results (Fig. 3) shows that the spectral positions and shapes of the above resonances are clearly modified by increasing the angle of incidence. Indeed, the quasiguided mode splits for nonzero polar angles of incidence in accordance with photon energy dispersion relations in Fig. 2(b). It is important to notice that these peaks show a similar spectral position behavior for TE and TM polarizations. It is noteworthy that quasiguided peaks are Fano-type resonances and have asymmetric shape (Figs. 3, 4). In contrast to quasiguided modes, the particle plasmon resonance is absent in TE polarization. Due to the absence of plasmon mode, spectral features in TE polarization are sharp.

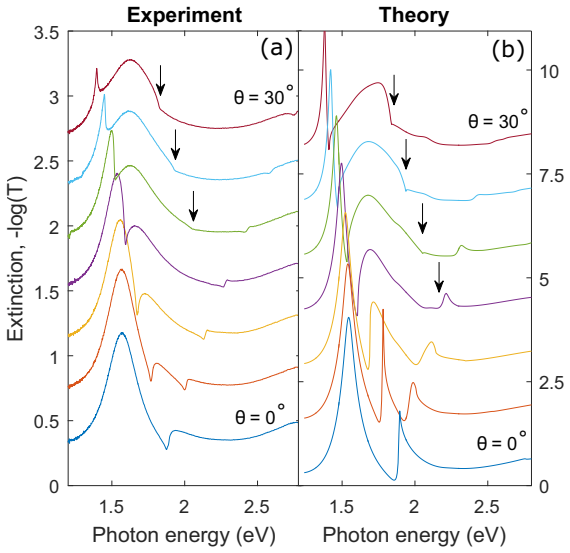


FIG. 3. Measured (left) and calculated (right) TM extinction spectra for light incidence with angle $\theta$ ranging from 0° to 30° in steps of 5°. Arrows show dips associated with Rayleigh anomalies.

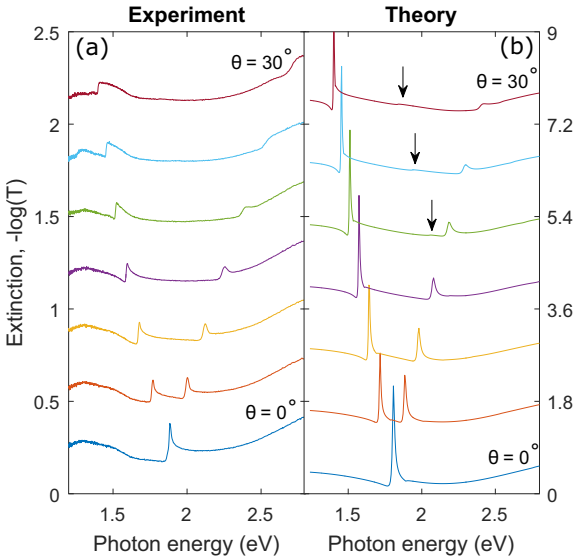


FIG. 4. Measured (left) and calculated (right) TE extinction spectra for light incidence with angle $\theta$ ranging from 0° to 30° in steps of 5°. Arrows show dips associated with Rayleigh anomalies.

Besides the quasiguided modes and the plasmon resonance, the extinction spectra in TM and TE polarizations have cusps that are poorly seen by a naked eye and are marked by arrows in Fig. 3. These are Rayleigh anomalies, which are well studied for metallodielectric structures. The spectral positions of these anomalies correspond to the vacuum light cone folded into the first Brillouin zone in Fig. 2(b). Physically, Rayleigh anomalies correspond to the opening of new diffraction orders.

For the exact interpretation of spectra in Figs. 3 and 4, the extinction of investigated structures was calculated as a two-dimensional function of frequency and the $x$ component of the momentum vector of incident light. Figures 2(c), 2(d) shows this function along with the positions of the above described peaks in the experimental extinction spectra. One can see that the position of the resonances is in agreement with the photon energy dispersion relations obtained the in empty lattice approximation [Fig. 2(a)]. In TM polarization, due to strong coupling between the quasiguided mode and nanowire plasmon, there is a strong anticrossing behavior of the modes instead of their spectral overlap. The corresponding Rabi splitting between upper and lower waveguide-polariton branches is about 100 meV.

### C. Field distributions

The above analysis of the extinction spectra suggests that the geometry of the sample induces the strong coupling between two photonic resonances, namely, the localized surface plasmon and the quasiguided mode. In general, the coupled resonance system is characterized by its normal (renormalized) frequencies and partial (non-normalized) frequencies. In order to understand the origin of the resonances, we calculate the electromagnetic near-field distribution in the structure.

We will limit our discussion to the normal angle of incidence $\theta = 0$ and zero azimuthal angle $\phi = 0$. The calculated

spatial electric field distributions in TM polarization are shown in Fig. 5 for $\hbar\omega = 1.55$ eV, 1.86 eV, and 1.90 eV, which correspond, respectively, to the two extinction maxima and the extinction minimum (see Fig. 3, the lowermost curve). It can be seen from Fig. 5(a) that the electric field at $\hbar\omega = 1.55$ eV is mainly localized inside the nanowires and clearly demonstrates the dipolar plasmon resonance. A field modulation coefficient, i.e., the ratio between the maximal and minimal electric field intensities over the period of electromagnetic oscillation, is of the order of 80. Due to a large distance between the neighboring wires, the near-field interaction between them can be neglected. In case of the extinction minimum ($\hbar\omega =$ 1.86 eV), the electric field avoids nanowires nearly completely. This mode takes the shape of vortices located between the gold nanowires and the $SiO_2$ substrate and represents the quasiguided mode. The field modulation coefficient for this mode is equal to 5. Finally, the electric field $\hbar\omega = 1.90$ eV, possess the features of both the plasmon mode and the quasiguided mode and the modulation coefficient is of the order of 80. Our simulations revealed that at all three photon energies, the time difference between the part at which electric and magnetic fields becomes maximal is approximately a quarter of the oscillation period. Hence, the field distributions, shown in Fig. 5, correspond, in the main, to standing waves.

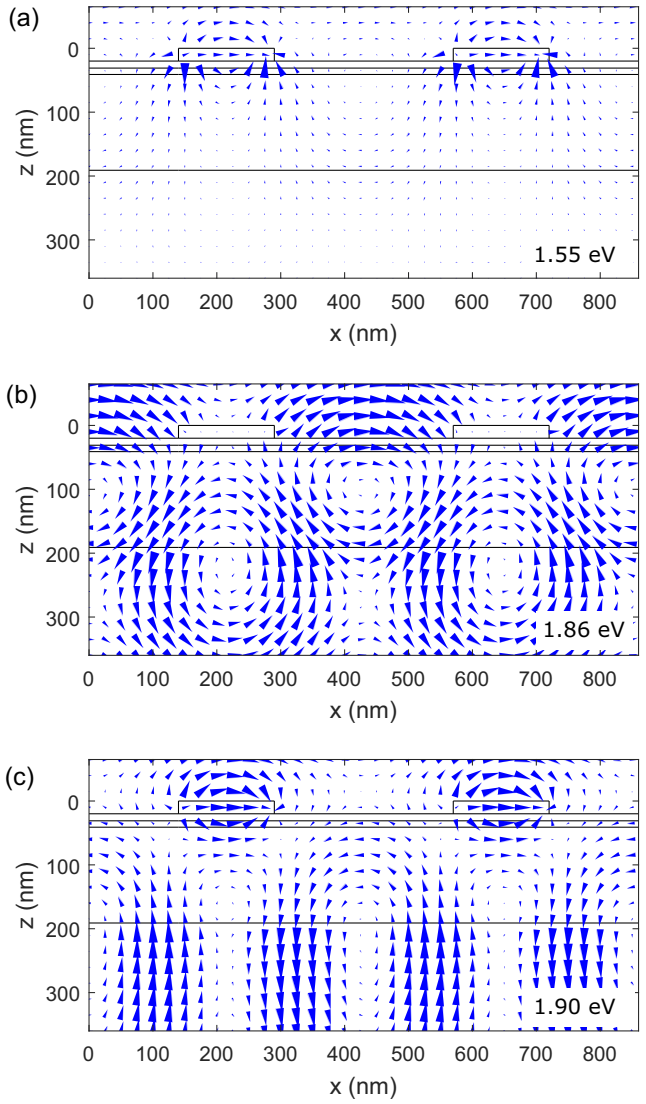


FIG. 5. Calculated spatial distributions of the electric field in the structure with silicon nanocrystals for normal incidence of TM polarized light. The fields are shown for the photon energy of (a) $\hbar\omega = 1.55$ eV, (b) $\hbar\omega = 1.86$ eV, and (c) $\hbar\omega = 1.90$ eV. The size of triangles is proportional to the field at the central point of each triangle. Triangles specify the corresponding electric field direction by their orientation. The fields are depicted at the instant time when the field intensities, integrated over the displayed cross sections, reach a maximum.

From the viewpoint of the coupled mode theory, the pure quasiguided character of the electric field at $\hbar\omega = 1.86$ eV is called as a dynamic damping effect; the corresponding frequency of electromagnetic oscillation is associated with the partial frequency of the quasiguided mode.

### D. Enhancement of PL intensity

As it is mentioned in Sec. I, the presence of metallic nanoparticles can drastically increase the photoluminescence intensity of semiconductor quantum dots. In our structures, the silicon nanocrystals are separated from the gold nanowires by a 20 nm ITO/$SiO_2$ buffer layer and, therefore, are almost not affected by localized surface plasmons. Therefore, in this study, we focus on the interaction of silicon nanocrystals with quasiguided modes.

From the above analysis of the electromagnetic resonances, it follows that when a plane wave traveling from the far field hits the corrugated sample at a certain angle it can couple to the quasiguided modes. Due to the electrodynamic reciprocity principle, a wave that propagates in the waveguiding layer can outcouple from the corrugated sample. In both cases the momentum conservation law is fulfilled due to the presence of grating, which folds all modes into the first Brillouin zone. This means that in our structure with gold grating, the photons being emitted by silicon nanocrystals at $\omega$ and $k_x$, which satisfy the dispersion relation of quasiguided mode, can resonantly come out from the sample [24]. In the structure that is not covered by grating, the photons with the same $\omega$ and $k_x$ are also emitted but they do not outcouple to the far field because in this case corresponding modes are entirely below the light cone [see Fig. 2(a)]. In other words, the waveguiding light cannot come out from the structure because its propagation angle is larger than the critical angle for air/substrate interface [27]. Therefore, in the corrugated structure the PL light is expected to overcome the critical angle limit and outcouple to the far field at certain frequencies and angles that correspond to the dispersion of the quasiguided modes (see Fig. 2).

The experimental PL spectra of the samples with silicon nanocrystals covered by gold grating are shown in Fig. 6. The PL spectra are normalized to those of the structures without grating (see inset in Fig. 6). In order to trace the dispersion, the PL spectra were collected at different angles between the PL light beam (determined by the vertical slit diaphragm) and perpendicular to the sample surface. One can see that at normal collection angle, the PL spectrum has single peak while for nonzero angles it splits into two. Only one peak can be seen in the PL spectra for angles of 7° and 10.5° due to

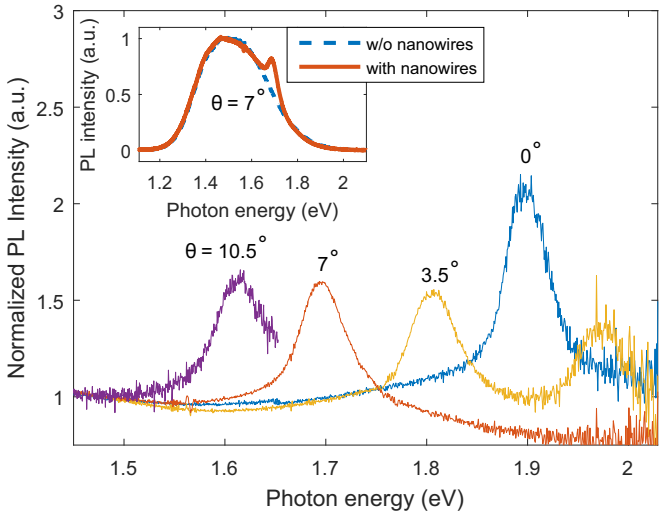


FIG. 6. The PL spectra of structures with silicon nanocrystals measured at different collection angles and normalized to those for structures without periodical gold grating. The comparison between normalized experimental PL spectra for structures with and without gold nanowires is shown in the inset.

the limited sensitivity of the experimental setup. With increase of the collection angle, the visible peak shifts to the lower energies. Note that the magnitude of the PL intensity from Fig. 6 exceeds 1, which denotes the enhancement in PL signal from silicon nanocrystals in the structure with periodicity.

The theoretical PL spectra in TM and TE polarizations for normal angle of collection is shown in Fig. 7 along with the theoretical extinction spectra taken at normal angle of incidence. From Fig. 7 one can see that the emissivity maximum is red shifted with respect to the extinction maximum in full agreement with the experimental results (see Fig. 3, Fig. 4, and Fig. 6).

Theoretical emissivity peaks are narrower and stronger than their experimental counterparts. This originates from

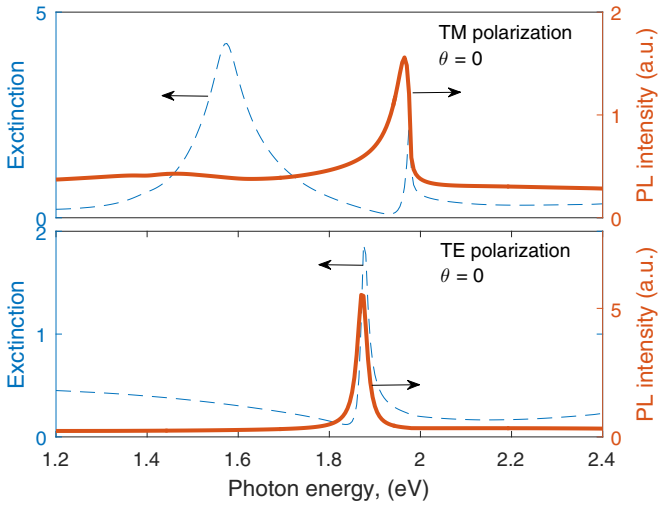


FIG. 7. Emissivity spectrum (red solid line) and extinction spectrum (blue dashed line) calculated at (a) TE polarization and (b) TM polarization for normal angle of incidence.

uncontrolled processes of absorption and diffuse scattering due to the deviation of the fabricated samples from the theoretical model. Usually such imperfections can be accounted for by phenomenological increase of the extinction coefficients of the materials. We do not use this approach because in this work we are mainly focused on the spectral position of the resonances rather than their $Q$ factors.

Due to the above-mentioned absorption and scattering, and also due to the fact that the spectral positions of the resonance peaks in TM and TE polarizations differ only by about 5%, it appears impossible to experimentally distinguish between two linear polarizations. Indeed, both polarizations were measured, however, no significant difference was detected.

The two-dimensional dependence of emissivity on the photon energy and the $x$ component of the wave vector is shown in Figs. 2(e), 2(f). From Figs. 2(e), 2(f) it can be seen that the angular dependence of emission intensity follows the dispersion relation of quasiguided modes. The energy dispersion of the resonances can be approximately described by the relation

$$E(k) = \frac{\hbar c}{n_{\text{eff}}} \left| k_x + \frac{2\pi m}{a} \right|, \tag{3}$$

where $n_{\text{eff}}$ is the effective refractive index of the guided mode and $m$ is an integer. The resonance peak of emissivity at normal collection angle corresponds to twofold degenerate ($m = \pm 1$) state in the $\Gamma$ point. The degeneracy of this state is lifted at $k_x \neq 0$.

## IV. CONCLUSION

In conclusion, we have shown experimentally and theoretically that gold nanowire grating can strongly influence the optical properties of silicon nanocrystals in the substrate. The measured transmission spectra of such photonic crystal structure are in a qualitative agreement with the simulation results obtained by the scattering matrix method. The extinction spectra are characterized by sharp peak due to the excitation of lossy quasiguided mode in the layer with silicon nanocrystals. The appearance of these modes leads to enhancement of photoluminescence intensity at the corresponding photon energies. We have shown that the PL light, being emitted by silicon nanocrystals, couples to the standing wave of the quasiguided mode and then leaves the sample.

## ACKNOWLEDGMENTS

This work was supported in part by the Russian Foundation for Basic Research (Grants No. 15-32-21153, No. 14-02-00778). A.M. acknowledges support from EU project ICONE (Grant No. 608099).

[1] K. Konishi, M. Nomura, N. Kumagai, S. Iwamoto, Y. Arakawa, and M. Kuwata-Gonokami, Circularly Polarized Light Emission from Semiconductor Planar Chiral Nanostructures, Phys. Rev. Lett. **106**, 057402 (2011).

[2] S. Noda, M. Fujita, and T. Asano, Spontaneous-emission control by photonic crystals and nanocavities, Nature Photon. **1**, 449 (2007).

[3] P. Lodahl, A. F. Van Driel, I. S. Nikolaev, A. Irman, K. Overgaag, D. Vanmaekelbergh, and W. L. Vos, Controlling the dynamics of spontaneous emission from quantum dots by photonic crystals, Nature (London) **430**, 654 (2004).

[4] S. V. Lobanov, T. Weiss, N. A. Gippius, S. G. Tikhodeev, V. D. Kulakovskii, K. Konishi, and M. Kuwata-Gonokami, Polarization control of quantum dot emission by chiral photonic crystal slabs, Opt. Lett. **40**, 1528 (2015).

[5] J. Biteen, L. Sweatlock, H. Mertens, N. Lewis, A. Polman, and H. Atwater, Plasmon-enhanced photoluminescence of silicon quantum dots: Simulation and experiment, J. Phys. Chem. C **111**, 13372 (2007).

[6] R. J. Walters, J. Kalkman, A. Polman, H. A. Atwater, and M. J. A. de Dood, Photoluminescence quantum efficiency of dense silicon nanocrystal ensembles in $Sio_2$, Phys. Rev. B **73**, 132302 (2006).

[7] H. A. Atwater and A. Polman, Plasmonics for improved photovoltaic devices, Nature Mater. **9**, 205 (2010).

[8] J. S. Biteen, N. S. Lewis, H. A. Atwater, H. Mertens, and A. Polman, Spectral tuning of plasmon-enhanced silicon quantum dot luminescence, Appl. Phys. Lett. **88**, 131109 (2006).

[9] J. S. Biteen, D. Pacifici, N. S. Lewis, and H. A. Atwater, Enhanced radiative emission rate and quantum efficiency in coupled silicon nanocrystal-nanostructured gold emitters, Nano Lett. **5**, 1768 (2005).

[10] S. A. Dyakov, D. Zhigunov, A. Hartel, M. Zacharias, T. Perova, and V. Y. Timoshenko, Enhancement of photoluminescence signal from ultrathin layers with silicon nanocrystals, Appl. Phys. Lett. **100**, 061908 (2012).

[11] R. Ferre, B. Garrido, P. Pellegrino, M. Perálvarez, C. Garcia, J. Moreno, J. Carreras, and J. Morante, Optical-geometrical effects on the photoluminescence spectra of Si nanocrystals embedded in $SiO_2$, J. Appl. Phys. **98**, 084319 (2005).

[12] E. Takeda, T. Nakamura, M. Fujii, S. Miura, and S. Hayashi, Surface plasmon polariton mediated photoluminescence from excitons in silicon nanocrystals, Appl. Phys. Lett. **89**, 101907 (2006).

[13] S. Miura, T. Nakamura, M. Fujii, M. Inui, and S. Hayashi, Size dependence of photoluminescence quantum efficiency of si nanocrystals, Phys. Rev. B **73**, 245333 (2006).

[14] F. Iacona, G. Franzo, E. Ceretta Moreira, and F. Priolo, Silicon nanocrystals and Er[sup 3+] ions in an optical microcavity, J. Appl. Phys. **89**, 8354 (2001).

[15] J. Goffard, D. Gérard, P. Miska, A.-L. Baudrion, R. Deturche, and J. Plain, Plasmonic engineering of spontaneous emission from silicon nanocrystals, Sci. Rep. **3**, (2013).

[16] D. Kovalev, M. B. Chorin, J. Diener, F. Koch, A. L. Efros, M. Rosen, N. Gippius, and S. Tikhodeev, Porous Si anisotropy from photoluminescence polarization, Appl. Phys. Lett. **67**, 1585 (1995).

[17] D. V. Guzatov, S. V. Vaschenko, V. V. Stankevich, A. Y. Lunevich, Y. F. Glukhov, and S. V. Gaponenko, Plasmonic enhancement of molecular fluorescence near silver nanoparticles: theory, modeling, and experiment, J. Phys. Chem. C **116**, 10723 (2012).

[18] A. Zelenina, S. A. Dyakov, D. Hiller, S. Gutsch, V. Trouillet, M. Bruns, S. Mirabella, P. Löper, L. López-Conesa, J. López-Vidrier *et al.*, Structural and optical properties of size controlled si nanocrystals in $Si_3N_4$ matrix: The nature of photoluminescence peak shift, J. Appl. Phys. **114**, 184311 (2013).

[19] D. Hiller, A. Zelenina, S. Gutsch, S. A. Dyakov, L. López-Conesa, J. López-Vidrier, S. Estrade, F. Peiro, B. Garrido, J. Valenta, M. Korinek, F. Trojanek, P. Maly, M. Schnabel, C. Weiss, S. Janz, and M. Zacharias, Absence of quantum confinement effects in the photoluminescence of $Si_3N_4$-embedded si nanocrystals, J. Appl. Phys. **115**, 204301 (2014).

[20] S. V. Lobanov, T. Weiss, D. Dregely, H. Giessen, N. A. Gippius, and S. G. Tikhodeev, Emission properties of an oscillating point dipole from a gold Yagi-Uda nanoantenna array, Phys. Rev. B **85**, 155137 (2012).

[21] A. Christ, S. G. Tikhodeev, N. A. Gippius, J. Kuhl, and H. Giessen, Waveguide-Plasmon Polaritons: Strong Coupling of Photonic and Electronic Resonances in a Metallic Photonic Crystal Slab, Phys. Rev. Lett. **91**, 183901 (2003).

[22] A. Christ, T. Zentgraf, J. Kuhl, S. G. Tikhodeev, N. A. Gippius, and H. Giessen, Optical properties of planar metallic photonic crystal structures: Experiment and theory, Phys. Rev. B **70**, 125113 (2004).

[23] M. Zacharias, J. Heitmann, R. Scholz, U. Kahler, M. Schmidt, and J. Bläsing, Size-controlled highly luminescent silicon nanocrystals: A $SiO/SiO_2$ superlattice approach, Appl. Phys. Lett. **80**, 661 (2002).

[24] S. G. Tikhodeev, A. L. Yablonskii, E. A. Muljarov, N. A. Gippius, and T. Ishihara, Quasiguided modes and optical properties of photonic crystal slabs, Phys. Rev. B **66**, 045102 (2002).

[25] D. M. Whittaker and I. S. Culshaw, Scattering-matrix treatment of patterned multilayer photonic structures, Phys. Rev. B **60**, 2610 (1999).

[26] L. Li, Use of fourier series in the analysis of discontinuous periodic structures, JOSA A **13**, 1870 (1996).

[27] Strictly speaking, we can only speak about the critical angle when the $x$ projection of the momentum, $k_x$, and the frequency $\omega$ are above the light line in the material of the substrate. Otherwise, the angle of waveguiding light propagation in the substrate is mathematically purely complex, which makes the above interpretation confusing.